Δελτίο της Ελληνικής Γεωλογικής Εταιρίας, 2010
Πρακτικά 12ου Διεθνούς Συνεδρίου
Πάτρα, Μάιος 2010

Bulletin of the Geological Society of Greece, 2010
Proceedings of the 12th International Congress
Patras, May, 2010

IMPLEMENTATION OF A NON-SPLITTING FORMULATION OF PERFECTLY MATCHED LAYER IN A 3D – 4TH ORDER STAGGERED-GRID VELOCITY-STRESS FINITE-DIFFERENCE SCHEME

Skarlatoudis A.A[1], Papazachos C.B.[2]

[1] *Geophysical Laboratory, Department of Geology, University of Thessaloniki, Thessaloniki-Greece, askarlat@geo.auth.gr*

[2] *Geophysical Laboratory, Department of Geology, University of Thessaloniki, Thessaloniki-Greece, kpapaza@geo.auth.gr*

Abstract

One of the major problems in numerical simulations of wave propagation in elastodynamics using grid-point methods is the truncation of the computational space by artificial boundaries. These boundaries produce spurious reflections, polluting the results with artificial noise, therefore several efforts have been realized in order to achieve transparent or non-reflecting boundaries for truncating the computational space. Perfectly Matched Layer (PML) has been one of the most efficient methods for implementing artificial boundaries at the edges of the computational models. However the application of PML requires the "tuning" of several variables, for which very limited work has been presented. In the present study we employ the Non-Splitting formulation of PML (NPML) technique presented by Wang & Tang (2003), based on the introduction of small perturbations in the wavefield. The NPML formulation shows the same accuracy with the originally introduced PML but is easier to be implemented because it does not require the field splitting. The main scope of this paper is to perform a full analysis of the efficiency of NMPL based on numerical tests using a 3D–4th order staggered-grid velocity-stress finite-difference scheme. The analysis consists of direct, quantified comparisons with reference solution waveforms from a semi-analytical method (Discrete Wavenumber Method) with synthetic waveforms produced using the most popular Absorbing Boundary Conditions (ABCs) and PML, in various canonical models (homogeneous and layer over half-space).

Key words: *Finite-Difference, Perfectly Matched Layer, Non-Splitting Formulation.*

1. Introduction

Numerical methods which are employed for wave propagation problems are necessarily applied in bounded media, using artificial boundaries (e.g. grid planes without neighbor grid planes from one side). On these artificial boundaries the energy of the computation area needs to be absorbed. Two solutions have been proposed for this problem, namely the absorbing boundary conditions (ABCs) and the absorbing layers. Berenger (1994) introduced an absorbing layer in 2-D and later (Berenger, 1996) in 3-D time domain electromagnetic numerical simulations, which he named (PML), since it had the property of being perfectly "matched" with the computation area medium. This means that at the bulk medium - absorbing layer interface, no spurious reflections were produced, while the

transmitted waves inside the layer were perfectly absorbed. PMLs have been eventually implemented in other scientific domains, such as computational acoustics and elastodynamics.

In elastodynamics, PMLs were first formulated for the P-SV case by Hastings et al. (1996) using compressional and shear potentials in the PML region. Since then, Chew and Liu (1996), Collino and Tsogka (2001), Festa and Nielsen (2003), Marcinkovich and Olsen (2003) amongst other researchers studied various aspects of PML properties. More Recently Komatitsch and Martin (2007) and Martin et al. (2008) presented an unsplit convolutional PML with improved performance at grazing incidence for purely elastic and poroelastic media.

Historically, the PML was formulated based on field splitting to avoid convolutional operations in the time domain. The Non-Splitting formulation of PML (NPML) uses perturbed equations to reduce automatically to the original wave equations in the inner layer, being equally efficient with PML and at the same time easier to implement. In the present work we use the NPML technique presented by Wang & Tang (2003), in order to perform a full analysis of the efficiency of NMPL using numerical tests with a 3D–4th order staggered-grid velocity-stress finite-difference scheme (Moczo et al., 2002, Kristek et al., 2002 and Kristek and Moczo, 2003). The analysis consists of direct comparisons of finite-difference synthetic waveforms with waveforms from discrete wavenumber method (DWN), which is used as a reference solution, for various canonical models (homogeneous and layer over half-space). Finally quantitative comparisons of synthetic waveforms produced using the most popular ABCs and PMLs for the same canonical models are also presented, in an attempt to exhibit the superiority of the latter as an artificial boundary in numerical computations, especially when the PML parameters are properly optimized.

2. The Non-Splitting (NPML) Formulation

The Non-Splitting formulation is essentially based on a coordinate stretching technique. Assume $p \in \{x,y,z\}$, the following coordinate transformation is defined:

(1)

where $p \in \{x,y,z\}$ are the transformed (stretched) coordinates, i is the imaginary unit and ω the angular frequency. Functions Ω_p are the attenuating functions in the PML zone, which depend on the layer thickness, the material velocity, the theoretical reflection coefficient and some additional constants. The properties of these functions and typical values of the theoretical reflection coefficient and constants used will be examined later in this work.

After coordinate stretching, the modified nabla operator is given by equation:

(2)

and the corresponding equation of motion becomes:

(3)

where ϱ is density, $\vec{V}$ is the velocity vector t is time and the stress vector. After applying the Fourier

Transformation, equation (3) yields

(4)

which after some algebra leads to equation:

(5)

Applying the inverse Fourier Transformation to equation (1) we obtain

(6)

If we define the following convolutional operator:

(7)

the inverse Fourier Transformation of equation (5) yields

(8)

Time derivative of Hooke's law for elastic media is given by equation

(9)

where $\{x, y, z, t\}$ is the stress tensor $\{x, y, z, t\}$, is the strain tensor and **c** is the elastic coefficients tensor. In the frequency domain equation (9) becomes

(10)

The relation between strain and the particle velocity field, $\vec{v}$ (x, y, z, t) is given by equation:

(11)

By applying again the coordinate stretching technique according to equation (1) and after taking into account equation (11), equation (10) becomes

(12)

where *u, v,* and w are the three velocity components.

After applying the inverse Fourier Transformation to previous equation (12) leads (after rearranging), to:

(13)

Since equation (13) involves time derivatives, can be expressed also as:

(14)

which is the most often used NPML formulation (Wang and Tang, 2003).

3. Implementation on NPML in a 3D-4th Order Staggered-grid Velocity-Stress Finite-Difference Scheme

The NPML formulation has been incorporated in the 3D–4th order staggered-grid velocity-stress finite-difference scheme proposed by Moczo et al. (2002). More information on this scheme can be found in Kristek et al. (2002) and Kristek and Moczo (2003). In this study we employed the time marching scheme by Wang and Tang (2003), using the trapezoidal rule (e.g. Davis and Rabinowitz, 1975), of 2nd order accuracy, for example:

(15)

where m is the time index, $P \in \{u, v, w\}$ and $p \in \{x, y, z\}$. In equation (15) functions Ω_p are the attenuating functions inside the PML layer. In the medium they are equal to zero, so the system of equa-

tions for velocity- stress NPML scheme is reduced to the original system of wave equations. Functions Ω_p are non-zero inside the PML layer, so that only waves propagating perpendicular to the PML plane are attenuated and consequently only the corresponding Ω_p functions have to be considered non-zero. For example, if a wave is propagating in the xz plane normal to x or z direction only Ω_x or Ω_z has to be computed, respectively. At the edges of the computational model (e.g of the xz plane) both and have to be computed. Different types of functions have been proposed by several authors for the attenuation, Ω_p, functions. In this work a slightly modified form of the function proposed by Collino and Tsogka (2001) were used, namely:

(16)

where δ is the thickness of the PML layer in grid points, p is the index of the current PML plane, V is the P-wave PML medium velocity, τ is a tuning variable and R the theoretical reflection coefficient. This theoretical reflection coefficient describes the desirable minimum reflection at the PML interface and is a function of the layer thickness (Collino and Monk, 1998a). This formulation shows the same accuracy with the originally introduced SPML but is easier to be implemented because it does not require the field splitting. In terms of computational efficiency the NPLM scheme used in this paper is equal to SPML, but in memory storage it is slightly less efficient than SPML since more variables have to be kept in core memory.

4. Numerical Testing Of The Non-Splitting PML Formulation

In order to numerically test the accuracy of NPML formulation, FD synthetics were compared using the Discrete Wavenumber method (DWN) (Bouchon, 1981; computer code Axitra Coutant, 1989). The comparisons were made for two different models, a homogeneous space and a surface layer over a homogeneous half-space. For the homogeneous model, calculations of synthetics were performed for two different values of V_p/V_s ratio, 4 and 1.78 (model A and B respectively), for examining the stability of the scheme in models with high velocity contrasts. For all types of models, a FD calculation was performed also for an enlarged version of each computational model, with the same source - receiver geometry but located far from the borders, in order to avoid any spurious reflections (reflection - free FD solution). A double-couple point source was used for all the FD computations. The source was simulated using a body-force term by a method suggested by Frankel (1993) and adapted for a staggered-grid by Graves (1996). A Gabor signal, was used as a source time function. Here, f_p is the predominant frequency, γ controls the width of the signal, θ is a phase shift and t_s=1. For testing both types of incident waves, two different values for the strike of the source were used (45° and 0°), in order to have "pure" P or S waves impinging on the PML boundary, according to the radiation pattern of a double-couple point source.

4.1 Homogeneous Model

The efficiency of PML for different incidence angles of the wavefield was tested in this model for both types of incident body waves. Models A and B have the same S wave velocity $\boldsymbol{\beta}$=562(m/s), density $\boldsymbol{\rho}$=2000 (Kg/m^3) and quality factors $\boldsymbol{Q_p}$=$\boldsymbol{Q_s}$=1000 and different P wave velocity $\boldsymbol{\alpha_A}$=2248(m/s) and $\boldsymbol{\alpha_B}$=1000(m/s). The size of the grid spacing h was determined using the rule that the minimum wavelength λ_{min} propagates in the grid with sufficient accuracy, must be six times larger than the grid

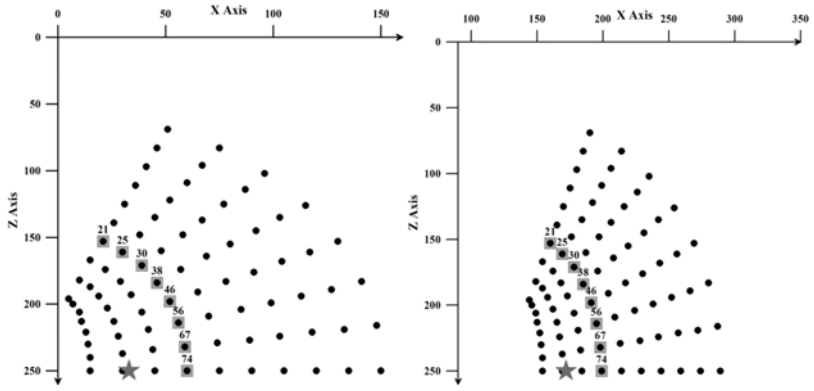

Fig. 1: Left: Source-receiver geometry for the incidence angle test. Black circles denote the position of receivers and stars show the source. With the light gray squares the receivers recordings plotted in Fig 2 are shown. Right: Source-receiver geometry for the enlarged model. The PML-inner medium interface is positioned at x=0 in both cases.

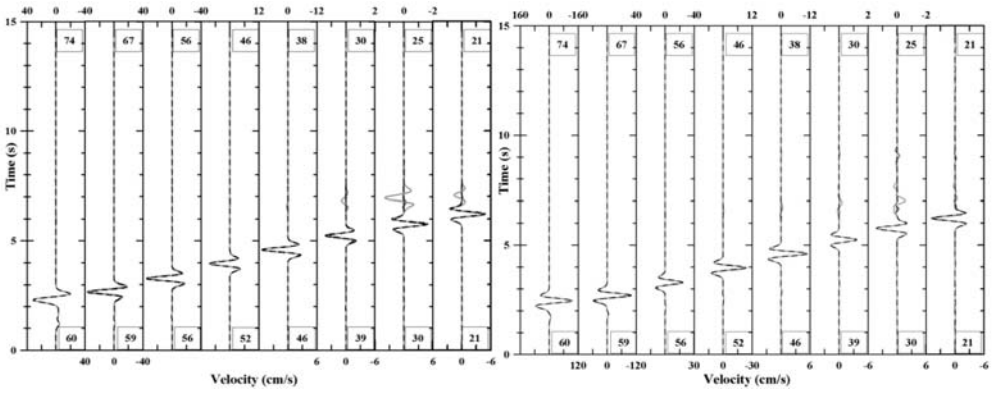

Fig. 2: Left: Longitudinal components of FD and DWN synthetics for model A and direct P waves incidence (left) and model B for direct S waves incidence (right). DWN synthetics are depicted with a black continuous line, FD synthetics with 30 grid-spacings PML thickness with a dark gray line, FD synthetics with 10 grid-spacings PML thickness with a light gray line and FD synthetics with 30 grid-spacings PML thickness for the enlarged model with a black dashed line. The numbers on top correspond to the number of the receiver plotted (Fig. 1), while numbers at the bottom correspond to the distance from the PML boundary in grid steps.

spacing ($h = \lambda_{min}/6$), which has been shown appropriate by stability and grid dispersion analysis in a homogeneous medium (Moczo et al., 2000). The number of grid cells of the computational models were *MX*=300, *MY*=300, *MZ* =500, the spatial grid spacing was *h*=30 m and the time steps for model A and B were dt_A=0.006 s and dt_B=0.013 s, respectively. For the enlarged models the number of grid cells for the incidence angle and surface tests were *MX*=350, *MY*=300, *MZ*=500 and *MX*=350, *MY*=350, *MZ*=400 respectively. The spatial grid spacing and the time steps for enlarged models (model A and model B) were the same.

4.2 Incidence angle test

The test was implemented using eight profiles of ten receivers each, which corresponded to eight in-

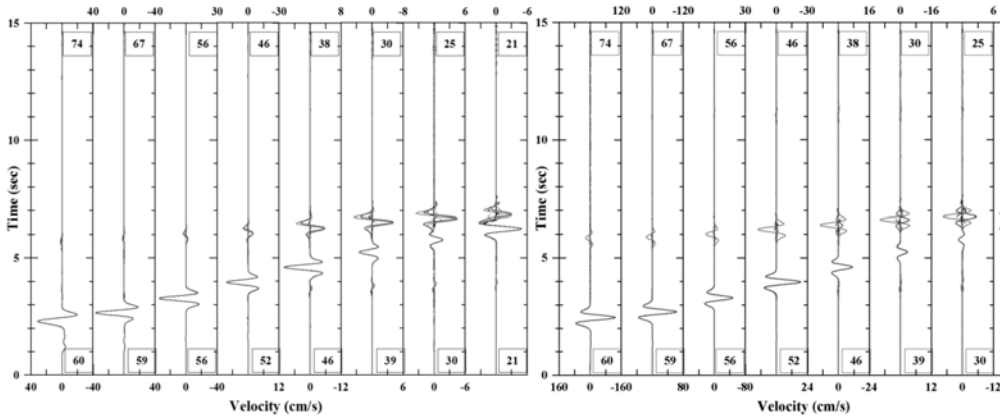

Fig. 3: Longitudinal components of FD and NRB synthetics for model A and direct P waves incidence (left) and for model B and direct S waves incidence (right). Coloring and numbering is described in the 3rd paragraph of current page.

cidence angles (0^0 to 70^0) with a step of 10^0 degrees. In Fig. 1 the configuration of source and receivers positions for the normal (left) and the enlarged (right) models are shown, respectively. The longitudinal components of the fourth receiver from the PML boundary of each profile (shown in Fig. 1) computed for direct incidence of P waves for model A and S waves for model B, are plotted in Figs. 2 together with the DWN synthetics. For receivers 74 and 78 no DWN synthetics were available because of intrinsic limitation of the method which does not allow computing solutions for receivers with equal depth or epicentre as the source.

In Fig. 2 DWN synthetics are depicted with a black continuous line, FD synthetics with a PML thickness of 30 grid spacings with a dark gray line, FD synthetics with a PML thickness of 10 grid spacings with a light gray line and FD synthetics for the enlarged model with a black dashed line.

4.3 Comparison with non-reflecting boundaries

The efficiency of PML comparing to other, commonly used, non-reflecting boundaries (NRB) was also tested for the previously described models. Five non-reflecting boundaries were used in these comparisons, namely Clayton and Engquist (1977), Higdon (1991), Peng & Toksöz (1994, 1995) and a combination of the first-order operator of Higdon (1991) with the A1 condition of Clayton and Engquist (1977) as implemented by P.-C. Liu and R. J. Archuleta (Moczo et al., 2002).

The computations were performed with the same source-receiver geometry and source parameters described for models A and B. The FD calculations were performed again for ten and thirty grid steps PML thicknesses. The synthetic waveforms were compared with the DWN solutions and for the quantification of these comparisons the single value envelope and phase misfits were calculated (Kristekova et al., 2006). In Fig. 3 the longitudinal components of the waveforms produced for all the non-reflecting boundaries, together with the 10 and 30 PML FD solutions for model A and direct P waves (left) and for model B and direct S waves (right) incidence are shown.

The 30 and 10 PML FD solutions are depicted with the sparse and dense black dashed lines, respectively, while the FD solutions for the enlarged model are shown with the black solid line. The solutions computed with the use of A1 condition of Clayton and Engquist (1977) and the Higdon (1991) operator are denoted with dark and light gray solid lines, respectively. The Peng & Toksöz

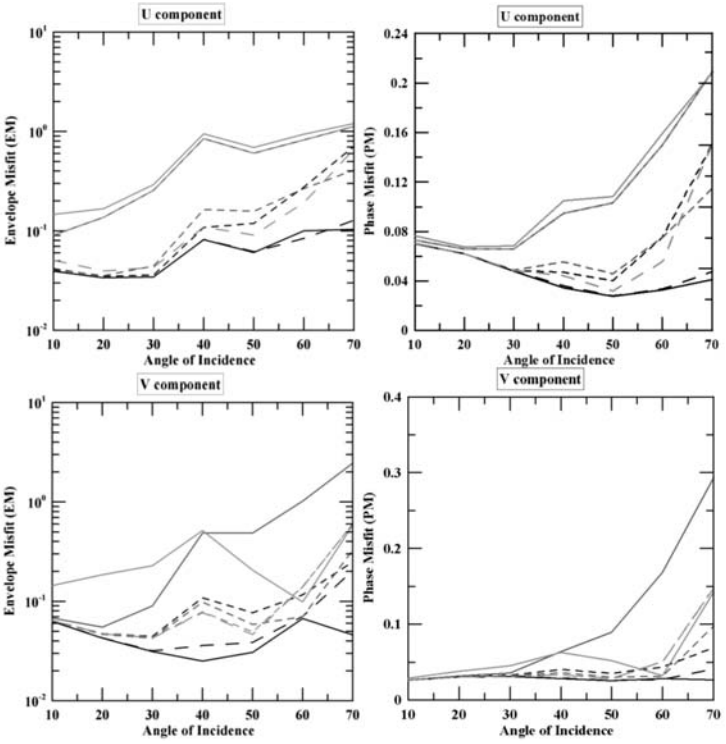

Fig. 4: Envelope and phase misfits for the horizontal component of FD and NRB synthetics for model A and direct P waves incidence (top) and for model B and direct S waves incidence (bottom). DWN synthetics are depicted with a black continuous line, FD synthetics with 30 grid-spacings PML thickness with a dark gray line, FD synthetics with 10 grid-spacings PML thickness with a light gray line and FD synthetics with 30 grid-spacings PML thickness for the enlarged model with a black dashed line.

(1994, 1995) solutions, for maximum attenuation set for the perpendicular displacement component of the P and S waves, are shown with the sparse and dense dashed light gray lines, respectively. Finally, the solution computed with the P.C. Liu and R. J. Archuleta non-reflecting boundary is denoted with the dense dark gray dashed line. Results from all comparisons performed, are quantified in Fig. 4, where the single value envelope and phase misfits are plotted against the incidence angle for the longitudinal components of both (A and B) models. The envelope misfit verifies the visual inspection of the calculated waveforms, with a noticeable diminished efficiency of the PML boundaries in the vicinity of the critical incidence angle and generally for grazing incidence angles.

Furthermore, envelope misfits are higher for model A than model B for the horizontal component, which might be an indication that PML can perform better than other non-reflecting boundaries in models with high Poisson ratios. Finally, it can be noticed that the 10-grid PML performs slightly worse for direct S wave incidence in comparison to direct P wave incidence for both models A and B, which suggests the need of thicker PML zones in cases that S waves are arriving at the computational model boundaries.

Phase misfits have much smaller values than the envelope misfits. This is strong indication that the errors introduced in the FD solutions from PML and other non-reflecting boundaries in general, are mostly due to changes in the amplitude and not in the phase of the waveforms. Phase misfits do not

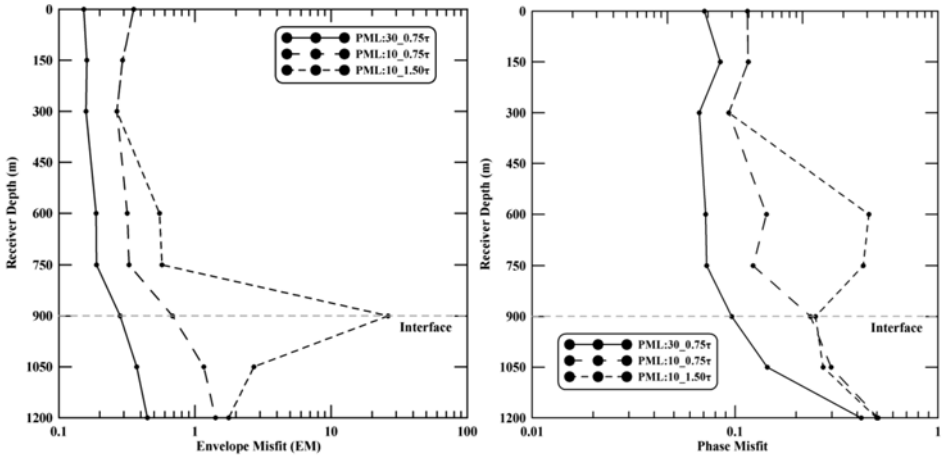

Fig. 5: Average envelope and phase misfits of the three components of each receiver plotted against receiver's depth for the LHS model.

exhibit the same trend as the envelope misfits becoming smaller with increasing incidence angles for the longitudinal component. Furthermore, on the contrary to amplitude misfits, phase misfits seem to be independent of the velocity contrasts or the type of the impinging wave.

4.4 Layer over half-space model

The second model used to test the efficiency and the overall behavior of NPML is a surface layer over a half-space (LHS) model. The size of the grid spacing h is the same determined and used for the homogeneous models (h=30 m). The number of grid cells in the x, y, and z directions are MX=400, MY=400, and MZ =300 and the time step dt=0.002 s. A double-couple point source with the same Gabor signal as a source time function was used for the FD computations in LHS model.

The test was implemented by using nine equidistant receivers positioned parallel to the Z axis, normal to the free surface. The first receiver was located at the free surface, while the deepest receiver at the depth of 1200 m. Moreover the seventh receiver was placed exactly on the layer – half-space interface in order to examine the behavior of the NPML in the vicinity of this internal boundary. The source was placed at a point with Cartesian coordinates (300, 4500, 450) m.

FD calculations were performed for ten and thirty grid steps PML thicknesses and two different values of the tuning variable τ [0.75, 1.5]. For the 3rd receiver no DWN synthetics were available due to the intrinsic limitation of the DWN method previously mentioned.

The single value envelope and phase misfits were calculated for the horizontal and vertical components of all receivers, using as a reference solution the DWN synthetics when possible. In Fig. 5 the averaged envelope and phase misfits for the three components of each receiver are plotted against the receiver's depth for all three combinations of PML thicknesses and τ values.

From these figures, the trend of thicker PML zones to produce better results can be observed, while the 10 grid-spacings PML zone performs better for lower values of the tuning variable τ (=0.75). Moreover the decreased efficiency of PML in the vicinity of the layer – half-space interface should be pointed out for all combinations of zone thicknesses and tuning variable values. Small phase misfits for all computations are also consistent with the results drawn from the homogeneous models, showing that NPML affect mostly the amplitude of the waves.

5. Conclusions-Results

The performance of a NPML technique was tested for the Cartesian coordinate system, as implemented for a 3D-4th order staggered-grid velocity-stress Finite-Difference scheme. Numerical tests were performed for investigating its overall performance in a layer over half-space and homogeneous half space models with high and low Poisson ratios. The results were compared with the semi-analytical solution provided by the Discrete Wavenumber Method (DWN) and quantified using a single value envelope and phase misfit, in order to study the influence of the NPML not only on the amplitude, but also on the phase of the impinging waveforms.

In all tests the Non-Splitting formulation did not exhibit instability problems in any of the models used (high and low Poisson ratios, LHS). NPML performance appeared to be better at almost vertical incidence angles and is reduced at grazing angles. Moreover their efficiency for the critical angle of incidence depends on the PML thickness. The trivial conclusion that thicker PML zones result in weaker artificial reflections was deducted from all the tests performed. For computations with high accuracy demands, a thicker PML zone is suggested (30 grid-spacings), providing that the memory cost from the thickest PML zone is affordable.

The comparison of the NPML with other, commonly used, Non-Reflecting boundaries is clearly in favor of PML. The envelope and phase misfits calculated, for any PML thickness and for all incidence angles exhibited systematically lower values. The higher efficiency of PML is shown for both horizontal components. Envelope misfits are higher for model A than model B, suggesting that PML perform better than non-reflecting boundaries in high Poisson ratios models. The poorer performance of 10-grid PML zones in direct S wave incidence comparing to direct P wave incidence for both models A and B might be related with the choice of the wave velocity used in Eq. (16). After several tests performed the P wave instead of S wave velocity was preferred, resulting in better and more stable results.

Phase misfits exhibit much smaller values than the envelope misfits. This is a strong indication that the errors introduced in the FD solutions from PML and other non-reflecting boundaries are mostly due to changes in the amplitude and not in the phase of the waveforms.

The artificial reflections in thinner PML zones are probably due to the boundary used for the termination of the PML zone. On the contrary, for thicker PML zones artificial reflections are probably caused by the finite contrast in properties between successive grid nodes, suggesting that the discrete PML zones behave almost as solid bodies. Stronger attenuation will enhance the contrast in properties of successive nodes for thicker zones while for thinner zones will produce stronger reflections from the PML interface. Thus the optimum solution should be based on a compromise between the thickness of the zone and the applied attenuation between successive nodes.

6. Acknowledgments

We would like to thank Dr. Ivo Oprsal for his helpful review and comments which improved the quality of the manuscript.

7. References

Berenger, J., (1994). A perfectly matched layer for the absorption of electromagnetic waves: *J. Comput. Phys.*, 114, 185–200.

Berenger, J. P. (1996). Three-dimensional perfectly matched layer for the absorption of electromagnetic waves, *J. Comp. Phys.*, 127, 363–379.

Bouchon, M. (1981). A simple method to calculate Green's functions for elastic layered media, *Bull. Seism. Soc. Am.*, 71, 959–971.

Chew, W., and Q. H. Liu, (1996). Perfectly matched layers for elastodynamics: a new absorbing boundary condition, J. Comp. Acoust., 4, 341–359.

Clayton, R., and B. Engquist, (1977). Absorbing boundary conditions for acoustic and elastic wave equations, *Bull. Seismol. Soc. Am.*, 67, 1529 – 1540.

Collino, F., and P., Monk, (1998a). Optimizing the perfectly matched layer, *Comput. Methods Appl. Mech. Eng.*, 164, 157–171.

Collino, F., and C. Tsogka, (2001). Application of the PML absorbing layer model to the linear elastodynamic problem in anisotropic heterogeneous media, Geophysics, 66, 294–307.

Coutant, O. (1989). Program of numerical simulation AXITRA. Res. Rep. LGIT (in French), Universite Joseph Fourier, Grenoble.

Engquist, B., and Majda, A., (1997). Absorbing boundary conditions for the numerical simulation of Waves: *Math. Comp.*, 31, 629–651.

Festa, G. and S. Nielsen, (2003). PML Absorbing Boundaries, *Bull. Seismol. Soc. Am.*, 93, 891–903.

Frankel, A. (1993). Three-dimensional simulations of ground motions in the San Bernardino Valley, California, for hypothetical earthquakes on the San Andreas fault, *Bull. Seism. Soc. Am.*, 83, 1020–1041.

Graves, R. W. (1996). Simulating seismic wave propagation in 3D elastic media using staggered-grid finite differences, *Bull. Seism. Soc. Am.*, 86, 1091–1106.

Hastings, F., Schneider, J. B., and Broschat, S. L., (1996). Application of the perfectly matched layer (PML) absorbing boundary condition to elastic wave propagation, *J. Acoust. Soc. Am.*, 100, 3061– 3069.

Higdon, R. L., (1991). Absorbing boundary conditions for elastic waves, Geophysics, 56, 231-241.

Komatitsch D. and R. Martin (2007). An unsplit convolutional perfectly matched layer improved at grazing incidence for the seismic wave equation, *Geophysics*, 72, 155–167.

Kristek, J., P. Moczo, and R. J. Archuleta, (2002). Efficient methods to simulate planar free surface in the 3D 4th-order staggered-grid finite-difference schemes, *Studia Geophys. Geodet.*, 46, 355–381.

Kristek, J., and P. Moczo, (2003). Seismic wave propagation in viscoelastic media with material discontinuities — A 3D 4th-order staggered-grid finite-difference modeling, *Bull. Seismol. Soc. Am.*, 93, 2273–2280.

Kristekova, M., J. Kristek, P. Moczo and S.M. Day, (2006). Misfit criteria for quantitative comparison of seismograms, *Bull. Seismol. Soc. Am.*, 96, 1836-1850.

Marcinkovich C. and K. Olsen, (2003). On the implementation of perfectly matched layers in a three-dimensional fourth-order velocity-stress finite difference scheme, *J. Geophys. Res.*, 108, 2276 – 2292.

Martin R., D. Komatitsch, and A. Ezziani, (2008). An unsplit convolutional perfectly matched layer improved at grazing incidence for seismic wave propagation in poroelastic media, *Geophysics*, 73, 51–61.

Moczo, P., J. Kristek, and L. Halada (2000). 3D fourth-order staggered grid finite-difference schemes: stability and grid dispersion, *Bull. Seism. Soc. Am.*, 90, 587–603.

Moczo, P., J. Kristek, V. Vavrycuk, R. J. Archuleta, and L. Halada, (2002). 3D heterogeneous staggered-grid finite-difference modeling of seismic motion with volume harmonic and arithmetic averaging of elastic moduli and densities, *Bull. Seism. Soc. Am.*, 92, 3042–3066.

Peng, C. and M. N. Toksöz, (1994). An optimal absorbing boundary condition for finite difference modeling of acoustic and elastic wave propagation, *J. Acoust. Soc. Am.*, 95, 733-745.

Peng, C., and Toksoz, M., (1995). An optimal absorbing boundary condition for elastic wave modeling, *Geophysics*, 60, 296–301.

Wang, T., and X. Tang, (2003). Finite-difference modeling of elastic wave propagation: A nonsplitting perfectly matched layer approach, *Geophysics*, 68, 1749–1755.